Publication Year	2022
Acceptance in OA	2025-02-14T17:49:36Z
Title	Optical and X-ray GRB Fundamental Planes as cosmological distance indicators
Authors	Dainotti, M. G., Nielson, V., SARRACINO, Giuseppe, Rinaldi, E., Nagataki, S., Capozziello, Salvatore, Gnedin, O. Y., Bargiacchi, G.
Publisher's version (DOI)	10.1093/mnras/stac1141
Handle	http://hdl.handle.net/20.500.12386/35981
Journal	MONTHLY NOTICES OF THE ROYAL ASTRONOMICAL SOCIETY
Volume	514

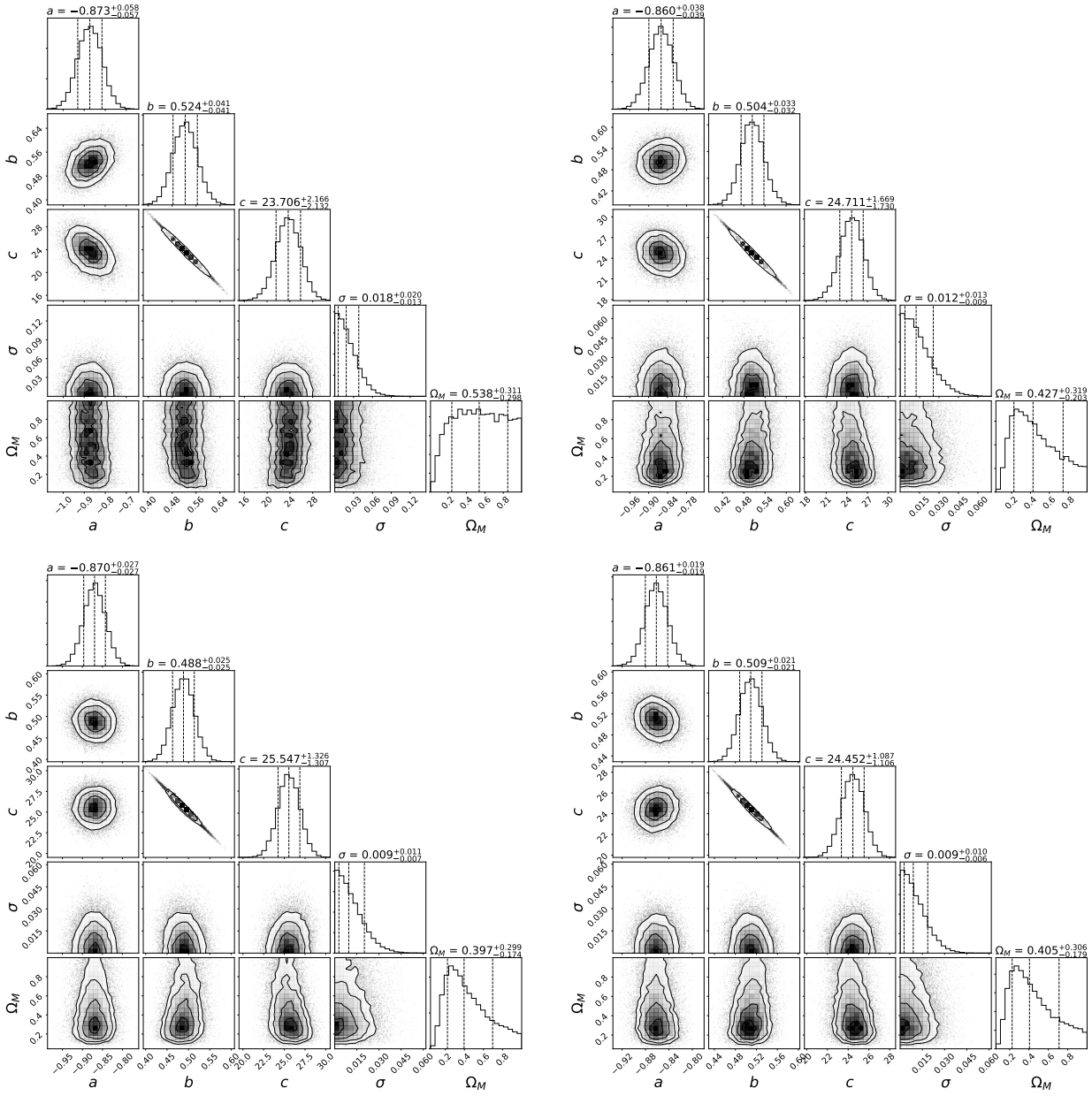

Figure 6. This figure shows the progression of closing contours around an Ω_M value for 50 (top left), 100 (top right), 150 (bottom left), and 200 (bottom right) GRBs simulated off the PLAT fundamental plane.

large of GRBs with halved error bars can be built in a relatively small amount of time due to the recent and rapid progression of efforts in the statistical reconstruction of GRB LCs, proving significant error bar reductions (Dainotti et al. 2022b). Dainotti et al. (2022b) tested that with the current sample a mean error reduction of 47.5% is viable with LC reconstruction (from now on called LCR) when we consider the error bars on the time at the end of the plateau, T_a and its correspondent flux. This is why we consider the scenario with confidence in this paper.

We now perform the same simulations and analysis on the full optical GRB sample. In Fig. 9, the upper panels show the convergence plots, the lower panels show the probability maps, and Fig. 10 shows for which number of simulated optical GRBs we reach the Conley et al. (2011), Betoule et al. (2014) and Scolnic et al. (2018) limits. These plots are surprising yet beneficial; despite a smaller sample size and increased σ_{int} on the optical fundamental plane, simulations using the full optical sample of 45 GRBs as a base produce clearly and abundantly more precise values for Ω_M than what the X-ray sample achieves. In fact, the optical sample with errors undivided trumps the X-ray sample with halved errors. The reason for this behaviour is still unclear and additional investigation alongside a larger sample is needed for a deeper explanation. The comparisons between the two wavelengths' results are showcased in Table 5. The optical sample proves itself to be 47.6% more precise than the X-ray sample

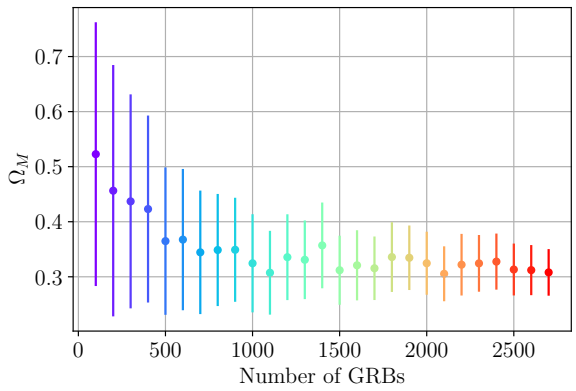

(a) X-RAY | Simulation Results for the Full PLAT Base with Undivided Errors

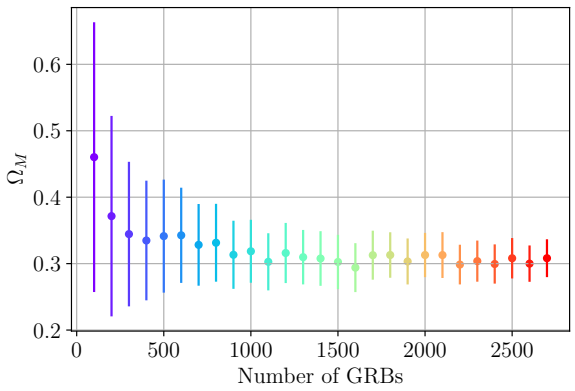

(b) X-RAY | Simulation Results for the Full PLAT Base with Halved Errors

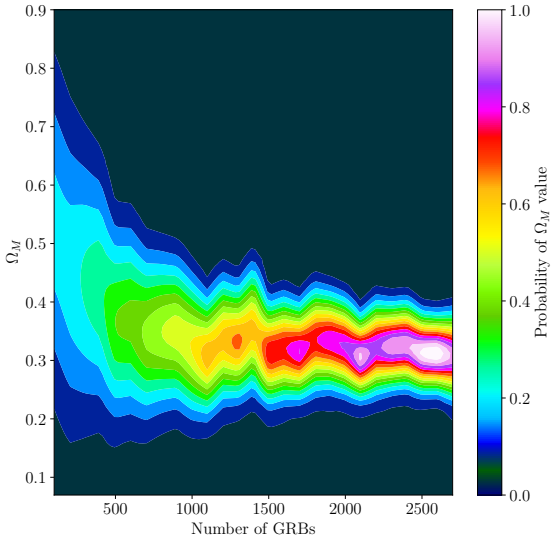

(c) X-RAY | Probability Map for Undivided Errors

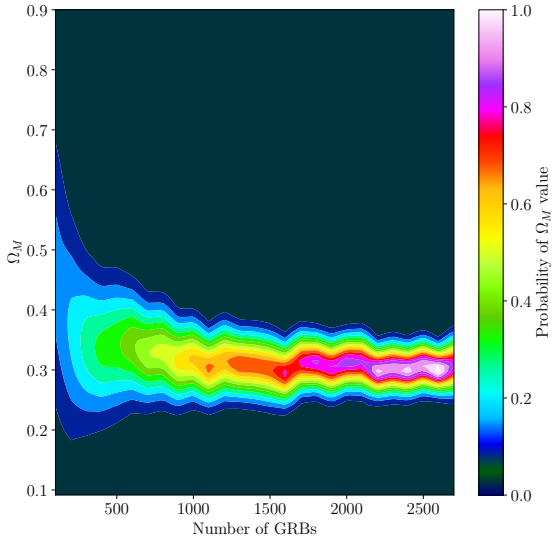

(d) X-RAY | Probability Map for Halved Errors

Figure 7. Upper left panel: the mean values of Ω_M vs. the numbers of GRBs obeying the X-ray fundamental plane to converge upon a value of Ω_M using GRBs as the standalone probe by considering the observed error bars. Upper right panel: the same as the left panel, but considering the error bars divided by 2. The bottom left and right panels show the corresponding probability distributions of the upper left and right panels, respectively.

when we consider n=1 and 44.4% for n=2 for 2700 simulated GRBs. Similarly, if we consider the cases with evolution the optical sample has a decrease in the scatter in determining Ω_M of 44.2% compared to the X-ray sample.

Furthermore, we find out from Fig. 10 that we only require 1031 optical GRBs to reach the Betoule et al. (2014) precision limit (left panel), and 284 when errors are halved (right panel). The Scolnic et al. (2018) limit is reached with 2718 and with 1086 GRBs for the undivided errors and divided by two errors scenarios, respectively (left and right panel of Fig. 10). We have extended this analysis by performing redshift evolution and selection bias corrections on the simulated GRBs in both wavelengths as was done in Sec.§5. However, as seen in Table 5, this correction results in less precise derivations of Ω_M. The behavior of the simulation results in general become less uniform in terms of convergence, as shown in Fig. 11. This is because we now must also consider the larger error bars on the evolutionary function slope for each variable.

Whereas before the optical samples provided the most precision, we find that after bias corrections, the X-ray GRB data remains the most reliable. This is because the slope of the optical evolutionary functions have larger uncertainties than their X-ray counterparts, given that the OPT sample is slightly smaller with a fundamental plane having a higher $\sigma_{\rm int}$.

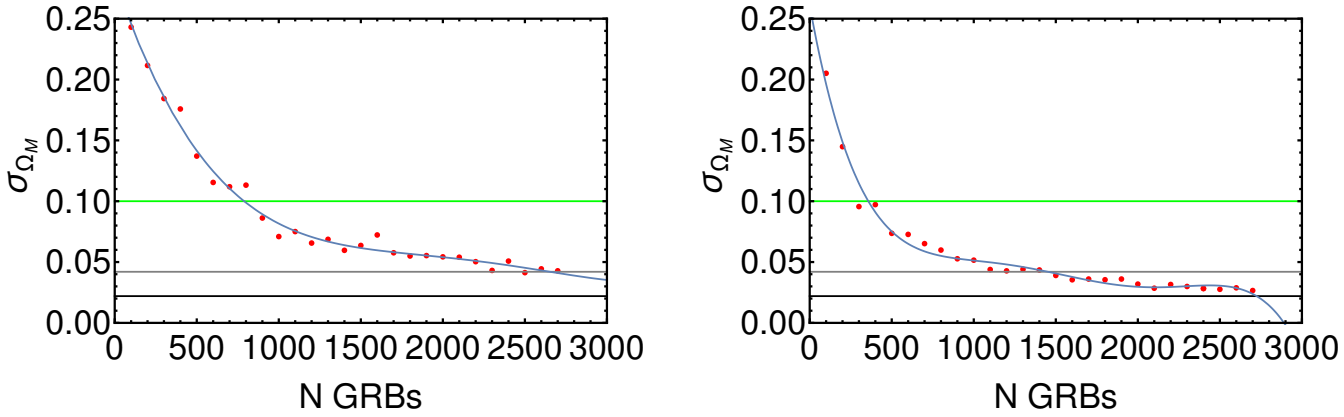

Figure 8. Left and right panels show the error plots for undivided and halved error bars, respectively, for the PLAT sample. The green, grey and black lines identify the Conley et al. (2011); Betoule et al. (2014) and Scolnic et al. (2018) errors on Ω_M, respectively. The blue line in the right panel denotes a polynomial fitting function used for the extrapolation.

Table 5. The first column is the X-ray and optical samples used, respectively, with "n" the number by which the sample errors are divided before entering the simulations. The second column is the number of GRBs. The third column shows the most probable value of Ω_M. The forth column is the standard deviation of the probability density functions correspondent to the numbers of simulated GRBs in the second column.

Sample	# GRBs	Most Probable Ω_M	σ_{pdf}
X-ray n = 1	2700	0.308 ± 0.042	0.037
Optical n = 1	2700	0.299 ± 0.022	0.018
X-ray n = 2	2600	0.300 ± 0.027	0.022
Optical n = 2	2600	0.301 ± 0.015	0.012
X-ray (EV) n = 1	2700	0.312 ± 0.052	0.043
Optical (EV) n = 1	2900	0.311 ± 0.029	0.023

Discussion on the methodology we employed to determine the error estimate on the MCMC sampler is drawn out in Appendix Sec. §A.

6.1 Simulated trimmed Samples as Increasingly Precise Cosmological Tools

We now explore ways of trimming the X-ray and optical samples to derive smaller error bars on the value of Ω_M than the ones derived by the full samples. The overall methodologies can indeed be repeated for future works as our observed sample sizes increase. First we use the 3D fundamental plane in X-ray as defined in Sec.§3.1 by the 10 GRBs that hold the intrinsic scatter of the plane near zero as a base for simulations.

By looking at the initial simulation results for a PLATtrim set of 10, we note a less smooth convergence than in the previous section where the full samples were instead used; fluctuating values are evident in Fig. 12. Although less uniform, the advantage to this model is that we do achieve smaller error bars than could be done with the full samples. In fact, it is by this trim in X-ray that we reach the smallest uncertainty yet with the X-ray sample for only 2300 GRBs (left panel of Fig. 13). All comparisons of the trimmed samples to the full samples in determining Ω_M are detailed in Table 6.

In addition to trimming the samples by those that hold the intrinsic scatter of the fundamental plane near-zero, we also choose to analyze an alternative method (called a posteriori) to the PLAT and OPT sample trimming to improve our results even further. We now run an array of simulations for varying PLATtrim and OPTtrim selections, looking for the number of GRBs used as a base for our simulations that optimizes our current sample. The criteria for which we consider a trimmed sample to be optimized follows from the computation of the smallest standard deviation on Ω_M for a given number of simulated GRBs. Although more time (and processor) expensive to test, this a posteriori sample trimming has potential to decrease the computed uncertainty significantly. We find that drawing from the full 50 X-ray and 45 optical GRBs, trimmed samples containing 20 and 25 GRBs, respectively, optimize our calculations. The plots from which we determined these values can be found in Appendix Sec. §B.

Fig. 12 compares the different trimmings and confirms our initial inference; although the trim done a priori with 10 GRBs (Fig. 12c) reduces uncertainties better than a posteriori trim with 20 GRBs, fluctuations in the a priori convergence exist already for n = 1. Therefore, when we choose to test n = 2, our a posteriori trimming choice (Fig. 12d) is more reliable. For details see Table

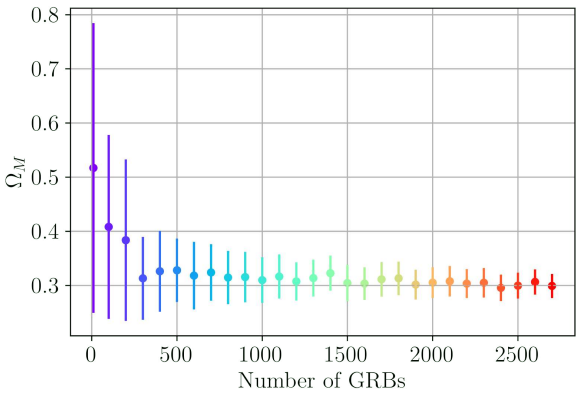

(a) OPTICAL | Simulation Results for the Full OPT Base with Undivided Errors

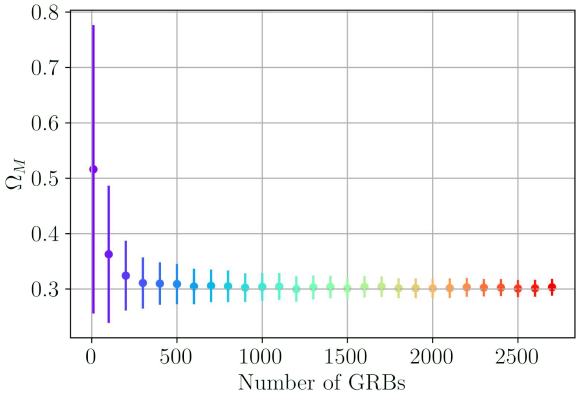

(b) OPTICAL | Simulation Results for the Full OPT Base with Halved Errors

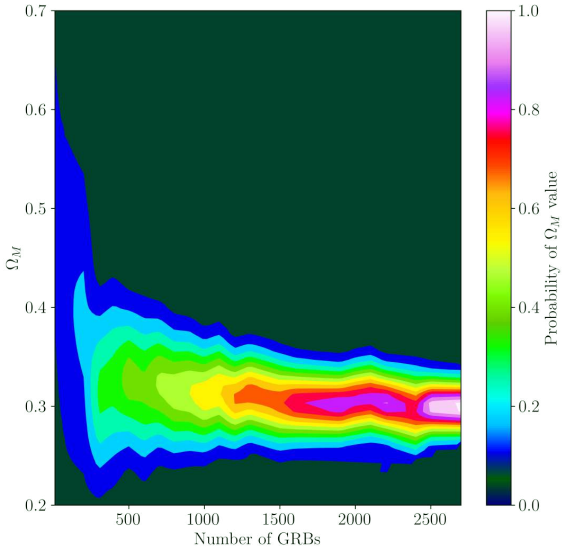

(c) OPTICAL | Probability Map for Undivided Errors

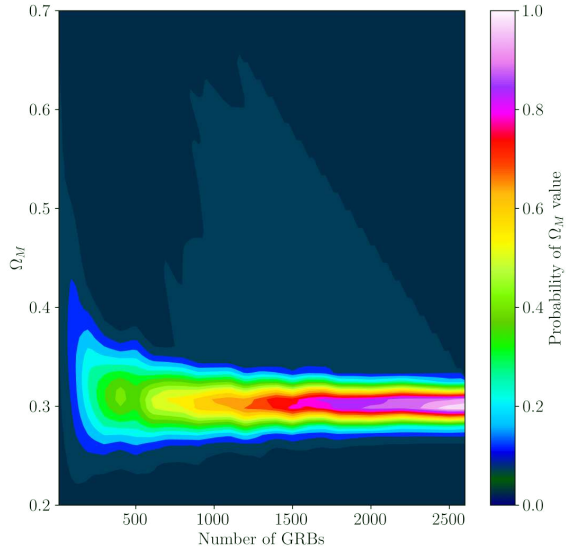

(d) OPTICAL | Probability Map for Halved Errors

Figure 9. Upper left panel: the mean values of Ω_M vs. the numbers of GRBs obeying the optical fundamental plane to converge upon a value of Ω_M using GRBs as the standalone probe by considering the observed error bars. The upper right panel: the same as the left panel, but considering the error bars divided by 2. The bottom left and right panels shows the corresponding probability distributions of the upper left and right panels, respectively.

6. The best estimates from these trims are depicted in Fig. 13. For both trims, the Conley et al. (2011), Betoule et al. (2014) and Scolnic et al. (2018) error limits are reached with a smaller number of GRBs. All error limit results can be seen in Table 7.

We find the smallest error bars, considering the optical sample, for an a posteriori-decided OPTtrim of 25 GRBs in both error division cases. And in fact, out of both wavelengths and trimming methodologies, this sample yields our best results yet in both error division scenarios and for three error limit definitions we considered in comparison with the literature (Fig. 14). We also note that in Table 6, for all instances of the optical GRB sample, we not only fall below the Betoule et al. (2014) standard deviation limit, but also near or even below the Scolnic et al. (2018) error limit (as again determined by SNe Ia only) of $\sigma = 0.022$. Scolnic et al. (2018) arrived at such a high precision using a large sample of 1048 SNe Ia, and the data we produce in the correspondent extrapolation (Fig. 15) suggests that, in the case of halved errors, we only need 36, 350 and 822 GRBs with plateaus to reach the Conley et al. (2011), Betoule et al. (2014) and Scolnic et al. (2018) limits, respectively. It is remarkable that the Conley et al. (2011) limit is already reachable now.

Taking this a posteriori approach to trimming, we re-run our previous computations involving the trimmed samples in both

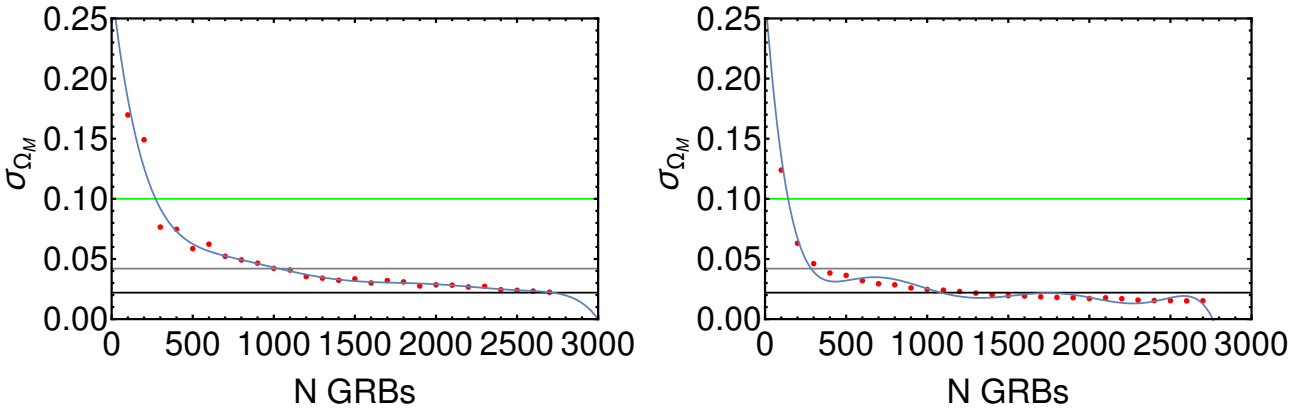

Figure 10. The plots show the number of simulated GRBs versus the error on Ω_M derived by the simulations starting from the full optical sample. On the left panel we have the undivided errors for the physical quantities related to the GRBs, while on the right panel we have divided these error by 2. The green, grey and black lines identify the Conley et al. (2011); Betoule et al. (2014) and Scolnic et al. (2018) errors on Ω_M, respectively.

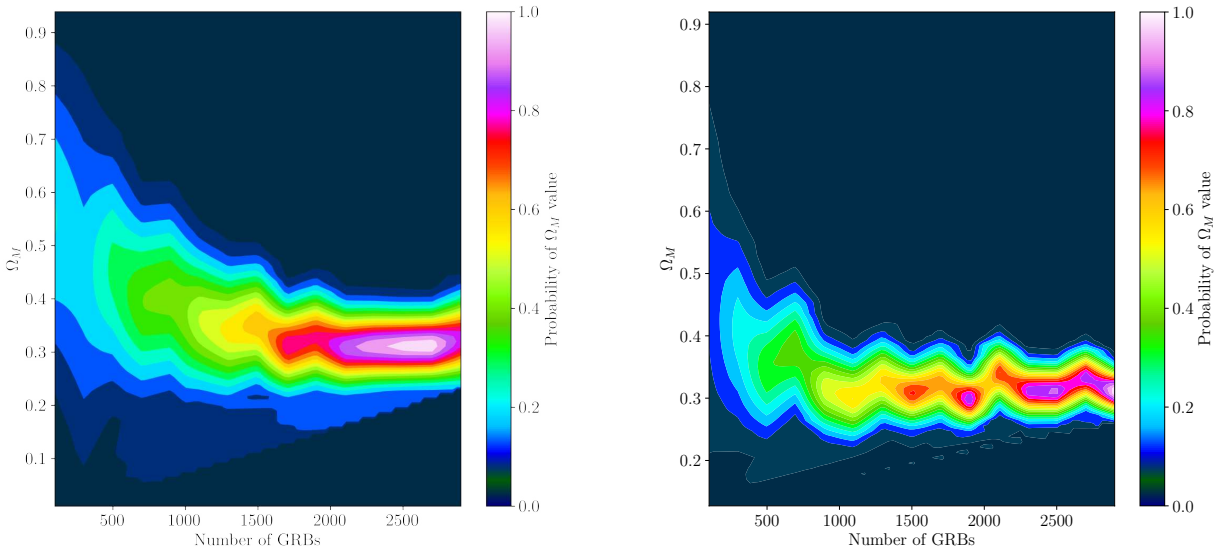

(a) X-RAY | Evolution-Corrected Probability Map

(b) OPTICAL | Evolution-Corrected Probability Map

Figure 11. The probability map for the X-ray (left panel) and optical (right) fundamental planes, both corrected for evolution.

wavelengths including SNe Ia data. These results are displayed in Table 8. We see no noticeable difference in either the values of Ω_M themselves, or in their uncertainties. We performed the same a posteriori trimming on the EV-corrected data, and similarly re-performed our computations considering the most efficacious cut of both wavelengths with SNe Ia. Therefore, we can conclude that the EV-corrected simulations presented in Table 8 below are the most precise derivations of the matter density of the Universe we can possibly achieve today given that the errors on Ω_M remain the same, but the treatment allow us to correct for selection biases and redshift evolution.

7 FUTURE DEEP-SPACE SURVEYS AND THEIR DETECTION POWER

Extrapolating minimum numbers of GRBs dependent upon error becomes useful in predicting which precision on Ω_M we can achieve in the future as current and future satellite missions observe increasingly detailed and more numerous data. One of these planned launches, studying X-ray emissions from GRBs, is the Space Variable Objects Monitor (SVOM, Wei et al. (2016)). The proposed launch date is June 2023, and it is to act as a pathfinder for a later mission, that is, the Transient High Energy Sources

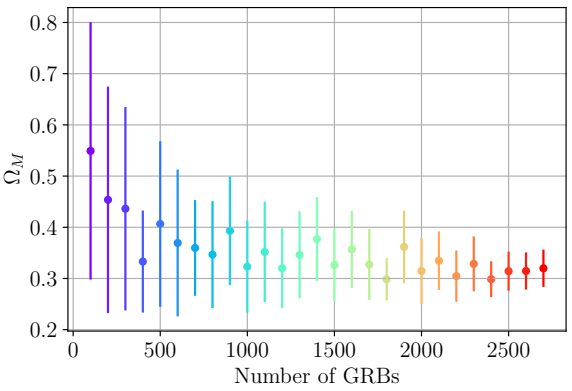

(a) X-RAY | Simulation Results for PLATtrim = 10 with Halved Errors

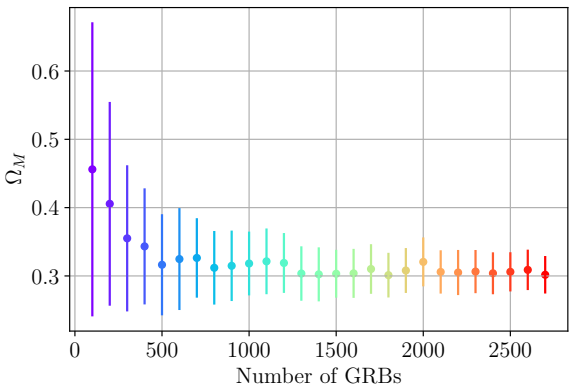

(b) X-RAY | Simulation Results for PLATTtrim = 20 with Halved Errors

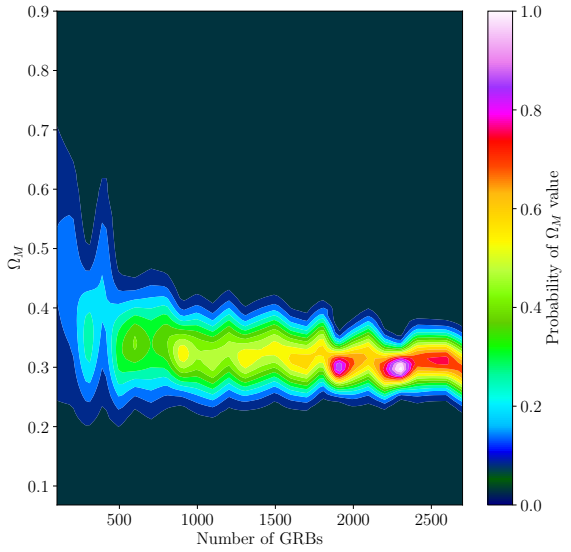

(c) X-RAY | Probability Map for PLATtrim = 10 with Halved Errors

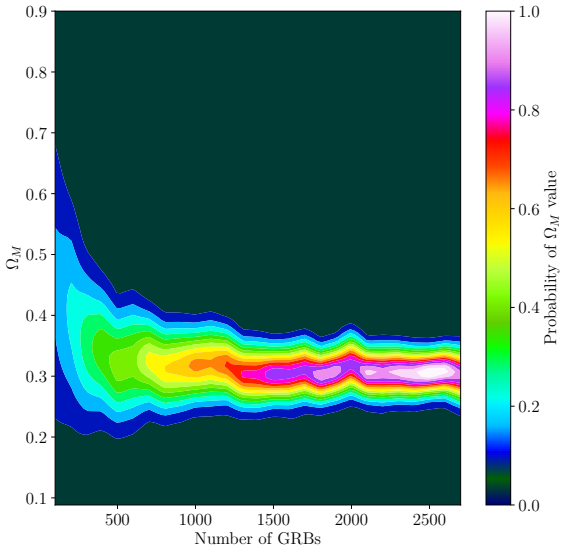

(d) X-RAY | Probability Map for PLATtrim = 20 with Halved Errors

Figure 12. Upper left panel: the mean values of Ω_M vs. the numbers of GRBs obeying the optical fundamental plane simulated with 10 GRBs. The upper right panel: the same as the left panel, but considering the plane simulated with 20 GRBs instead of 10. The bottom left and right panels shows the corresponding probability distributions of the upper left and right panels, respectively.

and Early Universe Surveyor (THESEUS, Amati et al. (2018)). SVOM is expected to detect around 80 GRBs per year, and for a planned three year mission, this means it should gather $\sim$ 240 GRBs throughout the course of its lifetime with $\sim 1-2$ triggers per week expected (Cordier et al. 2018).

SVOM's successor, THESEUS, has a very tentative launch date in 2037. Although the THESEUS mission has not been selected under Phase A study by ESA as a candidate M5 mission (Amati et al. 2021), there is the intent and the effort by the community to apply for other future funding schemes and opportunities. The number of expected GRBs triggers per year can reach up to 1000 (Amati et al. 2017). So one can expect up to three triggers per day (Frontera et al. 2018). THESEUS holds a hypothesized rate of GRB observation between 300-700 GRBs yr^{-1} (Amati et al. 2018).

We now use the calculated number of GRBs necessary to obtain ideal precision to predict, given the observing capability of both the present and the aforementioned future deep space survey missions, to estimate the length of time until X-ray and optical GRB emissions can be used in practice as standalone standard candles with limits on the errors on Ω_M comparable with the ones obtained using SNe Ia. Although the THESEUS team states that the mission will last for 3.45 years, we work under the assumption that its lifetime will be prolonged, as it has happened for many satellite missions. Specifically, we estimate its lifetime

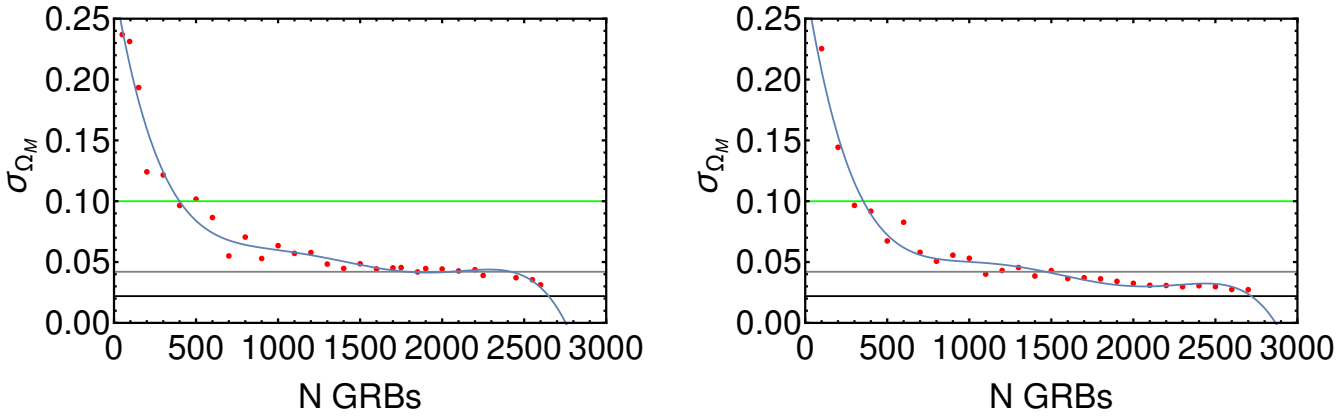

Figure 13. The plots show the number of simulated GRBs versus the error on Ω_M derived by the simulations. On the left panel we start from the PLAT sample trimmed with 10 GRBs and halved errors, while on the right panel we start from the PLAT sample trimmed with 20 GRBs and halved errors. The green, grey and black lines identify the Conley et al. (2011); Betoule et al. (2014) and Scolnic et al. (2018) errors on Ω_M, respectively.

Table 6. The first column shows the samples used, the second shows the number of GRBs used, with "n" the number by which the sample errors are divided before entering the simulations. A trimmed sample "a priori" refers to the sample of the 10 closest GRBs to their respective fundamental planes that yield an intrinsic scatter near-zero. The uncertainties reported are standard deviations. These results do not take into account redshift evolution or selection biases.

Sample	# GRBs	Ω_M
PLAT; n = 1	2700	0.308 ± 0.042
PLAT; n = 2	2600	0.300 ± 0.027
OPT; n = 1	2700	0.299 ± 0.022
OPT; n = 2	2600	0.301 ± 0.015
PLATtrim (a priori); n = 1	2400	0.299 ± 0.035
PLATtrim (a posteriori); n = 1	2400	0.300 ± 0.042
OPTtrim (a priori); n = 1	2900	0.306 ± 0.024
OPTtrim (a posteriori); n = 1	2700	0.305 ± 0.021
PLATtrim (a priori); n = 2	2300	0.299 ± 0.026
PLATtrim (a posteriori); n = 2	2700	0.302 ± 0.027
OPTtrim (a priori); n = 2	2600	0.301 ± 0.016
OPTtrim (a posteriori); n = 2	2600	0.301 ± 0.014
OPTtrim (a priori); n = 2	2900	0.300 ± 0.015
OPTtrim (a posteriori); n = 2	2900	0.299 ± 0.012

Table 7. The first column shows the sample, while the successive ones the numbers of GRBs needed for the limits set by Conley et al. (2011); Betoule et al. (2014), and Scolnic et al. (2018) for the full error bars and the halved ones. . We put an hyphen when the limit is not reached.

Number of GRBs with Plateaus Needed						
GRB Sample	Conley (2011)		Betoule (2014)		Scolnic (2018)	
	n = 1	n = 2	n = 1	n = 2	n = 1	n = 2
PLAT	789	357	2653	1452	-	2724
OPT	271	142	1031	284	2718	1086
PLATtrim (a priori)	847	399	2705	1788	2839	2649
OPTtrim (a priori)	330	112	829	393	2870	1513
PLATtrim (a posteriori)	646	354	2699	1466	-	2719
OPTtrim (a posteriori)	244	36	685	350	2104	822

to endure as long as the Konus-Wind mission, that has been in service for 27 years, or the Chandra X-ray Observatory, that is now almost 23 years old. Thus, our computation related to the lifetime of THESEUS for simplicity is posed to be 27 years. Given these estimates, the number of GRBs expected to be detected by THESEUS throughout the course of its mission is then 18900. By THESEUS, SVOM, and current rates of detection by Swift, we calculate the year in which the number of detected GRBs needed is achieved. The number of needed GRBs taken from the simulated data is listed as the number of GRBs with observed plateaus (# GRBs (Plateau)) in Tables 9 for the estimates to reach the limits of Conley et al. (2011) and Betoule et al. (2014) and Table 10 for reaching the limit of Scolnic et al. (2018). However, we must also consider that our PLAT sample of

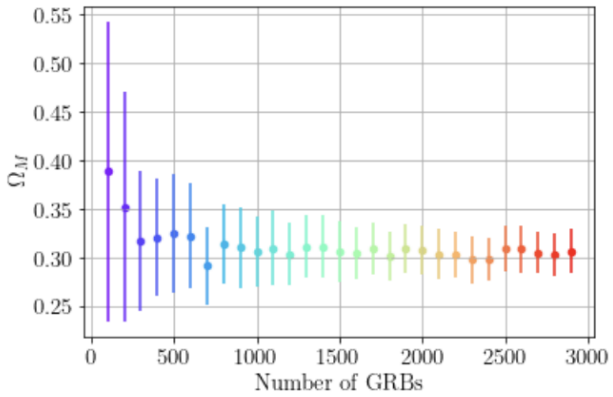

(a) OPTICAL | Simulation Results for OPTtrim = 25 with Undivided Errors

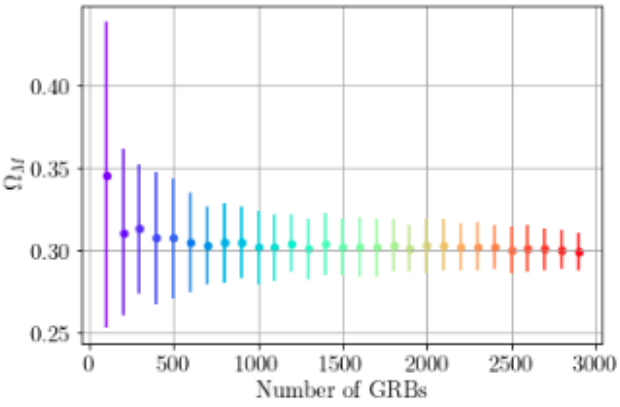

(b) OPTICAL | Simulation Results for OPTtrim = 25 with Halved Errors

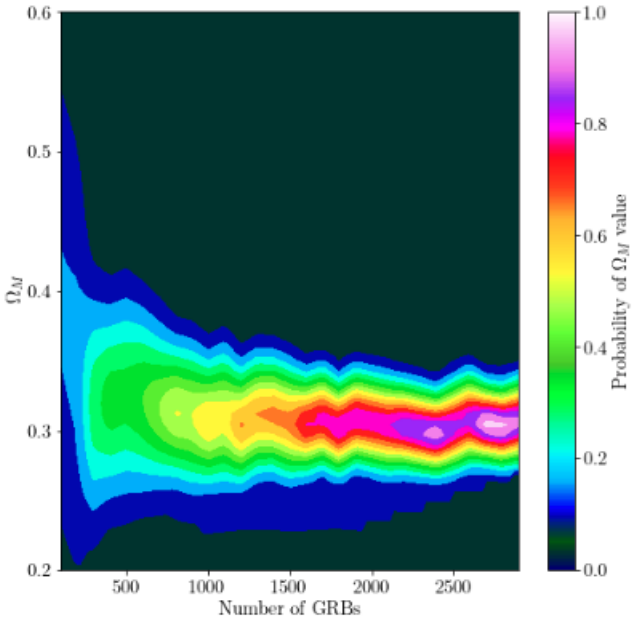

(c) OPTICAL | Probability Map for OPTtrim = 25 with Undivided Errors

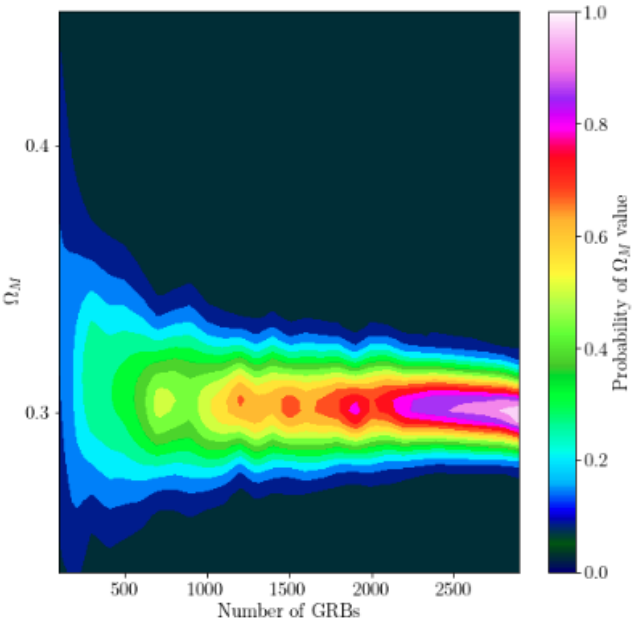

(d) OPTICAL | Probability Map for OPTtrim = 25 with Halved Errors

Figure 14. Upper left panel: the mean values of Ω_M vs. the numbers of GRBs obeying the optical fundamental plane simulated with 25 GRBs. The upper right panel: the same as the left panel, but considering the error bars divided by 2. The bottom left and right panels shows the corresponding probability distributions of the upper left and right panels, respectively.

Table 8. The first column shows the samples used, while the second shows the results on Ω_M with their errors, which are variances on the *emcee* chain, corresponding to the 68% confidence limit. The asterisk on the trimmed GRB sample indicates that it has been trimmed a posteriori. All fits are considering redshift evolution effects.

Sample	Ω_M
PLATtrim*+SNe Ia	0.299 ± 0.009
PLATtrim*+SNe Ia (EV)	0.299 ± 0.009
OPTtrim*+SNe Ia	0.299 ± 0.009
OPTtrim*+SNe Ia (EV)	0.299 ± 0.009

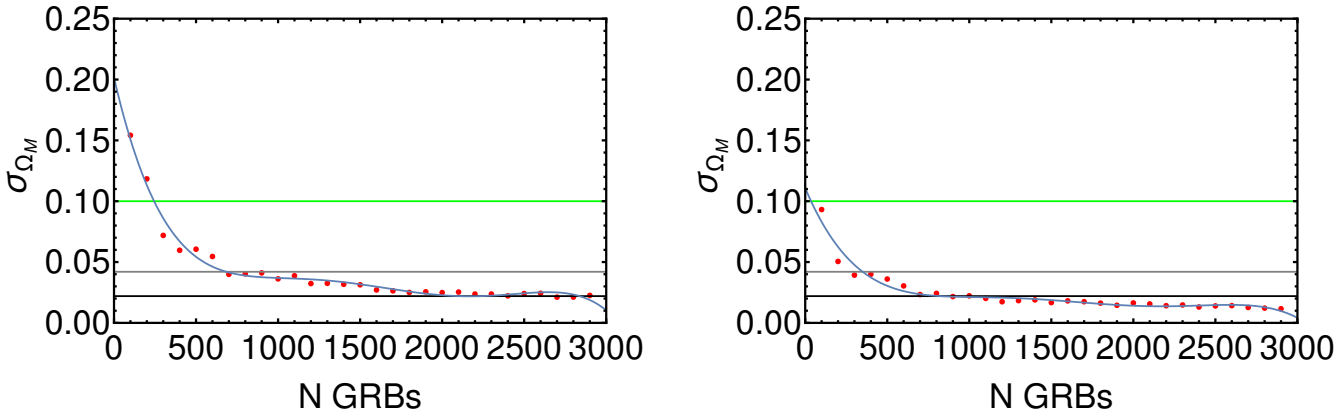

Figure 15. The plots show the number of simulated GRBs versus the error on Ω_M derived by the simulations. On the left panel we start from the optical sample trimmed with 25 GRBs (a posteriori) and undivided errors, while on the right panel we start from the same sample but with halved errors. The green, grey and black lines identify the Conley et al. (2011); Betoule et al. (2014) and Scolnic et al. (2018) errors on Ω_M, respectively.

Table 9. The first column shows all of the samples used. The three rows associated with each sample definition show the number of GRBs needed that have plateau phases, the total number of GRBs needed once the chosen sample proportionality out of the total samples are considered, and lastly, the year in which that number of GRBs is achieved with observed data. These rows are repeated for samples with the errors undivided, the errors halved, the errors undivided considering LCR, and finally, the errors halved including LCR. The overarching columns three and four give these estimates considering the precision reached by Conley et al. (2011) and Betoule et al. (2014), respectively. A sample "+ ML" implies that machine learning techniques are employed to double the initial sample size by redshift inference.

GRB Sample		Conley (2011)				Betoule (2014)			
		n = 1	n = 2	n = 1 (47.5% LCR)	n = 2 (47.5% LCR)	n = 1	n = 2	n = 1 (47.5% LCR)	n = 2 (47.5% LCR)
PLAT	# GRBs (Plateau)	789	357	374	169	2653	1452	1260	689
	# GRBs (Total)	16789	7596	7975	3608	56455	30898	26816	14676
	Year Achieved	2060	2044	2045	2037	2129	2085	2078	2056
PLAT + ML	# GRBs (Total)	8394	3798	3987	1804	28227	15449	13408	7338
	Year Achieved	2045	2037	2038	2026	2080	2058	2054	2043
OPT	# GRBs (Plateau)	271	142	128	67	1031	284	489	134
	# GRBs (Total)	4582	2401	2176	1140	17435	4802	8281	2281
	Year Achieved	2046	2038	2038	2026	2093	2047	2060	2038
OPT + ML	# GRBs (Total)	2291	1200	1088	570	8717	2401	4140	1140
	Year Achieved	2038	2027	2025	Now	2061	2038	2045	2026
PLATtrim (10)	# GRBs (Plateau)	847	399	402	189	2705	1788	1284	849
	# GRBs (Total)	18024	8490	8561	4033	57562	38048	27342	18073
	Year Achieved	2062	2045	2046	2038	2131	2097	2078	2062
PLATtrim (10) + ML	# GRBs (Total)	9012	4245	4280	2016	28781	19024	13671	9036
	Year Achieved	2046	2038	2038	2027	2081	2064	2054	2046
OPTtrim (10)	# GRBs (Plateau)	330	112	156	53	829	393	393	186
	# GRBs (Total)	5580	1894	2650	899	14019	6646	6659	3156
	Year Achieved	2050	2037	2039	2022	2081	2054	2054	2041
OPTtrim (10) + ML	# GRBs (Total)	2790	947	1325	449	7009	3323	3329	1578
	Year Achieved	2040	2023	2029	Now	2055	2042	2042	2032
PLATtrim (20)	# GRBs (Plateau)	646	354	306	168	2699	1466	1282	696
	# GRBs (Total)	13746	7533	6529	3578	57434	31196	27281	14818
	Year Achieved	2055	2044	2045	2037	2131	2085	2078	2057
PLATtrim (20) + ML	# GRBs (Total)	6873	3766	3264	1789	28717	15598	13640	7409
	Year Achieved	2043	2037	2036	2025	2081	2058	2054	2044
OPTtrim (25)	# GRBs (Plateau)	244	36	115	17	685	350	325	166
	# GRBs (Total)	4126	608	1959	289	11584	5918	5502	2811
	Year Achieved	2045	2018	2037	Now	2072	2051	2050	2040
OPTtrim (25) + ML	# GRBs (Total)	2063	304	979	144	5792	2959	2751	1405
	Year Achieved	2037	Now	2024	Now	2051	2040	2040	2030

GRBs is taken from the full 1064 GRBs presenting X-rays observed by Swift-XRT up until August 2019, and that our OPT sample is taken from the full 761 GRBs with optical observations from January 1997 - December 2018, including the ones without redshift measurements and detected plateaus. We must maintain these proportionalities when considering a minimum number of GRBs because our simulated sample must have an observable plateau emission phase and a detected redshift. So, more explicitly, we need to multiply the number of GRBs observable in X-rays by a factor of $\frac{1064}{50}$ (where 50 is the full PLAT sample) to compute how many GRBs with X-ray plateaus and with observed redshift will belong to the PLAT sample, and similarly by $\frac{761}{45}$ (where 45 is the full OPT sample) for the GRBs possessing an observed optical plateau with redshift. Multiplying by these ratios ensures that we account for these requirements. In addition, we need to consider the ratio of observations of the new missions. For clarity, we here summarize the assumptions and the rates underlying the forecasts of this section in bullet points:

- Lifetime of Theseus = 27 years, with an estimated launch in 2037.
- Lifetime of SVOM = 15 years, with an estimated launch in 2023.
- Total number of GRBs observed throughout the lifetime of THESEUS = 18900.
- Total GRBs observed throughout the lifetime of SVOM = 1350.
- Current rates of detection of Swift = 89.45 yr^{-1}.
- For X-ray wavelengths, we assume that the ratio (0.82) of the total number of GRBs observed by Swift-XRT (1064) from 2005 January until 2019 August compared to the total number of GRBs observed by Swift (1305) will be the same ratio of GRBs observed by the ECLAIRs (4-120 keV) on board of SVOM and the X-Gamma rays Imaging Spectrometer (XGIS, 2-20 MeV) and Soft X-ray Imager (SXI, 0.3-5 keV) on board of THESEUS.
- For optical wavelengths, we assume that the ratio (0.39) of the total number of optical afterglows (761) observed from 1997 up to December 2018, compared to the total number of GRBs by all missions (1942), is again the same as the one observed by the Infrared Telescope (IRT, 0.7-1.8 μm) on THESEUS, and as the Visible Telescope (VT, 540-600 nm) on board of SVOM.
- For optical wavelengths, we assume that additional ground-based instruments will also be operative as they are at this time. This is because, even if some of them will stop operating, we expect to have at least the same number and with the same capabilities as today from the ground based observations. We actually expect to have more, but we remain conservative in this estimate.

Keeping these assumptions and rates in mind, we define in Tables 9 and 10 a second column describing the total number of GRBs needed to achieve the error limit, considering both GRBs with and without plateau phases. We then calculate the year in which these simulated GRBs are predicted to be observed considering four types of GRB samples:

(i) all errors on the measured quantities undivided with no statistical reconstructions.
(ii) all errors halved with no statistical reconstructions.
(iii) all errors undivided initially, but by current LCR capabilities, 47.5% of the sample's errors are already halved.
(iv) all errors halved initially, and by current LCR capabilities, 47.5% of the sample's errors are halved again.

The year achieved is, of course, closer to the present for a simulated number of GRBs whose likelihood errors have been divided by two. As for the Betoule et al. (2014) limit, the earliest year in which we fall below the cutoff given current capabilities is in 2038 with the full OPT sample and 2056 for the full PLAT X-ray sample. It is in the decade or so that we expect to have enough observational data to use GRBs as standalone standard candles that produce errors on cosmological parameters less than or equivalent to those produced by SNe Ia measures. This time estimate is reduced, however, if we consider the applicability of current machine learning (ML) techniques including the LCR to effectively reduce the errorbars on the measurement of the fundamental plane relation and the redshift inference to double the PLAT sample of GRBs in X-ray that we can use for these calculations. Because such a small number of observed GRBs have had their redshift recorded ($\simeq \frac{1}{3}$), ML techniques have been developed by Dainotti et al. (2019) to estimate the missing redshifts. Indeed, it is possible to determine the redshift of GRBs possessing the plateau emission by completely non parametric models or semi-parametric models or a combination of the two. Considering also this research line, we find that we reach the full number of observed GRBs in X-ray necessary to use them as standard candles by 2026 for the Conley et al. (2011) limit, and by 2043 for the Betoule et al. (2014) limit. The limit found by Betoule et al. (2014) with the optical trimmed a posteriori (20 GRB) sample can be achieved much earlier, in 2025 (in just 3 years from now), using the ML techniques.
Furthermore, because of the particular efficacy of the OPTtrim sample in the constraint of Ω_M, we can estimate similarly the time frame in which the most recent and precise Scolnic et al. (2018) limit is achieved. From Table 10, considering both current statistical LCR and the redshift inference through the ML applications, GRBs will be just as ideal probes as SNe Ia reaching the Scolnic et al. (2018) limit in 2042, if we instead consider the limit of Betoule et al. (2014) we are able to reach it with LCR and redshift inference in just 4 years, in 2026. Both estimates are performed with the OPT trimmed a posteriori (25 GRBs).
We here point out that the value of Ω_M can be measured as a guide. This forecast, although based on the flat ΛCDM model,

Table 10. The first column shows all of the different optical GRB samples used. The three rows associated with each sample show the number of GRBs needed that have 1) plateau phases, 2) the total number of GRBs needed, and 3) the year in which that number of GRBs is achieved with observed data. These rows are repeated for samples with the errors undivided, the errors halved, the errors undivided considering LCR, and finally, the errors halved including LCR. These estimates are given considering the precision reached by Scolnic et al. (2018). A sample "+ ML" implies that machine learning techniques are employed to double the initial sample size by redshift inference.

GRB Sample		Scolnic (2018)			
		n = 1	n = 2	n = 1 (47.5% LCR)	n = 2 (47.5% LCR)
OPT	# GRBs (Plateau)	2718	1086	1291	515
	# GRBs (Total)	45964	18365	21833	8723
	Year Achieved	2197	2097	2140	2061
OPT + ML	# GRBs (Total)	22982	9182	10916	4361
	Year Achieved	2113	2063	2069	2046
OPTtrim (10)	# GRBs (Plateau)	2870	1513	1363	718
	# GRBs (Total)	48534	23054	12153	19840
	Year Achieved	2207	2123	2114	2074
OPTtrim (10) + ML	# GRBs (Total)	24267	12793	11527	6076
	Year Achieved	2118	2076	2072	2052
OPTtrim (25)	# GRBs (Plateau)	2104	822	999	390
	# GRBs (Total)	35580	13900	16900	6602
	Year Achieved	2159	2080	2091	2054
OPTtrim (25) + ML	# GRBs (Total)	17790	6950	8450	3301
	Year Achieved	2094	2055	2060	2042

can be generalized. In principle, we can use the fundamental plane for any cosmological model, and we don't need to restrict ourselves to a specific number of parameters. We can indeed use this data sample to constrain extended theories of gravity or more exotic cosmological models as well. The methodology that we have demonstrated is very general, and can be applied to any future cosmological model. The forecast in this particular paper is restricted to the flat ΛCDM model, and we are interested in constraining only Ω_M, as a benchmark quantity. Any additional forecasts are interesting, but beyond the scope of the current paper.

8 CONCLUSIONS AND INSIGHTS

In this paper, we have defined a subsample of 222 GRBs with redshift measurements and LC plateaus from all 1064 GRBs detected by Swift-XRT, and in combination with SNe Ia measurements, we have calculated the matter content of the Universe today to be $\Omega_M = 0.299 \pm 0.009$. We arrive at this precision using GRB emission data in optical wavelengths as well, marking a significant step in the recognition and usability of optical plateaus studies as cosmological tools. We have applied a procedure according to which a subsample of GRBs closer to the plane has been chosen, so that we could reduce the scatter of the fundamental plane at the smallest possible. The Sec. §2.1 results wherein we compare the distributions of the fluxes and times of the PLAT, OPT, PLATtrim and OPTtrim samples assert that picking a smaller number of GRBs does not bias the sample. The KS test shows that the hypothesis that the two samples are drawn by the same distribution cannot be rejected at the 5% level for all cases, but for the optical sample for T_a^*. We also stress here that the cosmological computations performed do not suffer of the circularity problem when we add GRBs and SNe Ia together GRBs are not calibrated over SNe Ia and do not assume any a priori cosmological models. We found that by trimming the X-ray sample to a sample of 10 (a priori) or 20 GRBs (a posteriori) in combination with SNe Ia leads to the same error as with the full PLAT sample. The results were as follows: $\Omega_M = 0.299 \pm 0.009$. For both GRB samples we account for redshift evolutionary effects using the EP methodology, thus achieving the smallest intrinsic scatter on the X-ray 3D fundamental plane in the literature to date, yielding a 44.4% reduction with respect to the one computed without considering these corrections. Employing this correction and retrieving the same value of Ω_M as stated above, we can be sure that this is the most precise determination of the density content yet. As was noted and is described in detail within the Appendix Sec. §A, all MCMC sampler errors have been quantified and determined to be an order of magnitude less than the order on which we compare the Ω_M symmetrized errors and standard deviations. This is the first time in which GRBs have been attempted to be used as standalone standard candles through simulations, with an inferred precision higher than the one obtained by SNe Ia samples alone once a sufficient number of simulated GRBs are accounted for. Because we do not currently

have enough GRB data to achieve this goal, we run MCMC simulations to define a probabilistic minimum number needed to satisfy them.

Simulating first using the full PLAT and OPT samples as the base, we find that a minimum of 150 GRBs is needed to provide closed-contours around an Ω_M value in our prior interval. However, to arrive at a desirable error on this value comparable to the limit set by SNe Ia, we instead simulate using as a base the PLATtrim and OPTtrim samples of 10 GRBs, because they yield intrinsic scatters near-zero. For instance, the PLATtrim gives a $\sigma_{\mathrm{int_{X,\,trim}}} = 0.05 \pm 0.05$ (right upper panel of Fig. 1), which is significantly less, 86% than that of the full PLAT, $\sigma_{\mathrm{int_{X,PLAT}}} = 0.36 \pm 0.04$ (left upper panel of Fig. 1), or even that of the evolution-corrected samples; PLAT (EV) yields $\sigma_{\mathrm{int_{X,PLAT,ev}}} = 0.20 \pm 0.06$ (44 % less than the PLAT), and PLATtrim (EV) gives $\sigma_{\mathrm{int_{X,trim,ev}}} = 0.13 \pm 0.09$ (64% less than the PLAT).

We aim to seek how many GRBs are needed to yield a value of Ω_M with a very high precision. For undivided errors on PLATtrim, the probability of $\Omega_M = 0.299 \pm 0.035$ approaches for 2400 GRBs (Table 6); in addition only 2705 X-ray GRBs are needed to reach the Betoule et al. (2014) standard deviation limit (Table 9). Instead, with undivided errors on OPTtrim, only 829 optical GRBs are needed. Because we have to consider the proportionality of the sample, these estimates must be increased to account for the presence of the redshift and the plateau in the sample. Therefore, in the attempt to decrease the GRBs numbers further, we explore alternative trimming techniques. By such, we trim both the optical and X-ray samples a posteriori and find more compelling uncertainties on the fundamental planes. Specifically, dividing the likelihood errors by two on PLATtrim (a posteriori) we find a most-probable $\Omega_M = 0.302 \pm 0.027$ for 2700 GRBs, and with halved errors on OPTtrim (a posteriori), we see a most-probable $\Omega_M = 0.299 \pm 0.021$ for 2700 GRBs (see Table 6). It is clear that the OPTtrim reaches an error bar on the Ω_M which is 22 % smaller compared to the one achieved by the PLAT with the same number of simulated GRBs. This allows to safely state that the OPTtrim is more efficacious than the PLATtrim.

We achieve the Betoule et al. (2014) limit with 1452 X-ray GRBs or 284 optical GRBs (see Table 9). We finally test for the more recent Scolnic et al. (2018) error cutoff of $\sigma = 0.022$, and find that the OPTtrim (a posteriori with 25 GRBs) sample can achieve this limit with 822 GRBs with plateau and halved error bars (see Table 10). Because of this, we look into deep-space survey missions that will be collecting this GRB data in coming years. By surveys such as SVOM, THESEUS, and the continued use of Swift, it is estimated that a number of 22486 GRBs will be gathered in their lifetimes. By factoring in the ability of machine learning techniques to derive redshifts and the successful halving of errors by the statistical reconstruction of GRB LCs (currently we can achieve this for 47.5% of a sample), we predict to arrive at the Scolnic et al. (2018) limit by 2042, and to the Betoule et al. (2014) limit with only 134 optical GRBs by 2026. This will be the time frame in which there will be enough observational data to effectively use GRBs as standalone standard candles, with SNe Ia comparable error deeming GRBs ideal cosmological probes.

These results are interesting because, as the definition of GRBs as standard candles becomes more and more reliable, the addition of these astrophysical objects to SNe Ia data will soon give the most precise derivation of Ω_M ever achieved. Furthermore, as it has been done previously (Dainotti et al. 2021a), we will also arrive at the most precise values for the dark energy parameter w, and for the Hubble Constant H_0. The inclusion of a larger X-ray PLAT sample or a platinum sample in optical to trim would decrease the intrinsic scatter of the plane even further and potentially lower our number of estimated GRBs. Not only this, but larger samples would allow for more constraining results on the redshift evolutionary effects. This would again increase the accuracies of our measurements. Furthermore, as we keep investigating the physics of GRB progenitors, we will be able to better define GRB classes, samples, and, thus, continue to improve the precision on our results as well as shed more and more light on the mechanism behind GRBs.

ACKNOWLEDGEMENTS

This work is supported by JSPS Grants-in-Aid for Scientific Research "KAKENHI" (A: Grant Number JP19H00693). This work was supported in part by a RIKEN pioneering project "Evolution of Matter in the Universe (r-EMU)". This work made use of data supplied by the UK Swift Science Data Centre at the University of Leicester. V. Nielson acknowledges the support by the United States Department of Energy in funding the Science Undergraduate Laboratory Internship (SULI) program. We are grateful to S. Savastano for the very preliminary help in writing the python codes for the simulations, and to N. Hornby, B. De Simone, A. Lenart, S. Young, N. O'Shea, D. Levine, N. Osborn, D. Zhou, and Z. Kania for running some of the computations here shown. We are also grateful to A. Lenart and D. Levine for running the Efron & Petrosian method on the optical and X-ray data. We also acknowledge the use of the RIKEN Hokusai BigWaterfall cluster for some of the simulations.

9 DATA AVAILABILITY

The data underlying this article will be shared upon a reasonable request to the corresponding author.

REFERENCES

Abbott T. M. C., et al., 2018, MNRAS, 480, 3879
Ajello M., et al., 2019, ApJ, 878, 52
Amati L., et al., 2002a, Mem. Soc. Astron. Italiana, 73, 1178
Amati L., et al., 2002b, A&A, 390, 81
Amati L., Guidorzi C., Frontera F., Della Valle M., Finelli F., Landi R., Montanari E., 2008, MNRAS, 391, 577
Amati L., O'Brien P., Goetz D., Tenzer C., Bozzo E., 2017, in Proceedings of the conference held 6-9 June 2017 in Rome I., ed., The X-ray Universe 2017. p. 250
Amati L., et al., 2018, Advances in Space Research, 62, 191
Amati L., D'Agostino R., Luongo O., Muccino M., Tantalo M., 2019, Monthly Notices of the Royal Astronomical Society: Letters, 486, L46–L51
Amati L., et al., 2021, arXiv e-prints, p. arXiv:2104.09531
Bargiacchi G., Risaliti G., Benetti M., Capozziello S., Lusso E., Saccardi A., Signorini M., 2021, Astron. Astrophys., 649, A65
Beaton R. L., Carnegie-Chicago Hubble Program Team 2018, in American Astronomical Society Meeting Abstracts #231. p. 351.05
Beniamini P., Duque R., Daigne F., Mochkovitch R., 2020, MNRAS, 492, 2847
Bernardini M. G., 2015, Journal of High Energy Astrophysics, 7, 64
Betoule M., et al., 2014, A&A, 568, A22
Birrer S., et al., 2020, A&A, 643, A165
Bloom J. S., Frail D. A., Sari R., 2001, AJ, 121, 2879
Boella G., Butler R. C., Perola G. C., Piro L., Scarsi L., Bleeker J. A. M., 1997, A&AS, 122, 299
Bromberg O., Nakar E., Piran T., Sari R., 2013, ApJ, 764, 179
Campana S., Guidorzi C., Tagliaferri G., Chincarini G., Moretti A., Rizzuto D., Romano P., 2007, A&A, 472, 395
Cannizzo J. K., Gehrels N., 2009, in American Astronomical Society Meeting Abstracts #213. p. 610.02
Cannizzo J. K., Gehrels N., 2010, in AAS/High Energy Astrophysics Division #11. p. 14.04
Cao S., Khadka N., Ratra B., 2021a, arXiv e-prints, p. arXiv:2110.14840
Cao S., Ryan J., Ratra B., 2021b, MNRAS, 504, 300
Cao S., Dainotti M., Ratra B., 2022, arXiv e-prints, p. arXiv:2201.05245
Capozziello S., Izzo L., 2008, Astron. Astrophys., 490, 31
Capozziello S., Izzo L., 2010, Astron. Astrophys., 519, A73
Capozziello S., Benetti M., Spallicci A. D. A. M., 2020, Foundations of Physics, 50, 893
Cardone V. F., Capozziello S., Dainotti M. G., 2009, MNRAS, 400, 775
Cardone V. F., Dainotti M. G., Capozziello S., Willingale R., 2010, MNRAS, 408, 1181
Carroll S. M., 2001, Living Reviews in Relativity, 4, 1
Chen Y., Kumar S., Ratra B., 2017, ApJ, 835, 86
Collazzi A. C., Schaefer B. E., Goldstein A., Preece R. D., 2012, ApJ, 747, 39
Conley A., et al., 2011, ApJS, 192, 1
Cordier B., Götz D., Motch C., SVOM Collaboration 2018, Mem. Soc. Astron. Italiana, 89, 266
Cucchiara A., et al., 2011, ApJ, 736, 7
D'Agostini G., 2005, arXiv e-prints, p. physics/0511182
Dainotti M., 2019, Gamma-ray Burst Correlations; Current status and open questions. Institute of Physics Publishing, doi:10.1088/2053-2563/aae15c
Dainotti M. G., Amati L., 2018, PASP, 130, 051001
Dainotti M. G., Del Vecchio R., 2017, New Astron. Rev., 77, 23
Dainotti M. G., Cardone V. F., Capozziello S., 2008, MNRAS, 391, L79
Dainotti M. G., Ostrowski M., Willingale R., 2011a, MNRAS, 418, 2202
Dainotti M. G., Cardone F. V., Capozziello S., Ostrowski M., Willingale R., 2011b, ApJ, 730, 135
Dainotti M. G., Cardone V. F., Piedipalumbo E., Capozziello S., 2013a, MNRAS, 436, 82
Dainotti M. G., Petrosian V., Singal J., Ostrowski M., 2013b, ApJ, 774, 157
Dainotti M., Petrosian V., Willingale R., O'Brien P., Ostrowski M., Nagataki S., 2015a, MNRAS, 451, 3898
Dainotti M. G., Del Vecchio R., Shigehiro N., Capozziello S., 2015b, ApJ, 800, 31
Dainotti M. G., Postnikov S., Hernandez X., Ostrowski M., 2016, ApJ, 825, L20
Dainotti M. G., Willingale R., Capozziello S., Cardone V. F., Ostrowski M., 2017a, AIP Conference Proceedings,
Dainotti M. G., Nagataki S., Maeda K., Postnikov S., Pian E., 2017b, A&A, 600, A98
Dainotti M. G., Hernandez X., Postnikov S., Nagataki S., O'brien P., Willingale R., Striegel S., 2017c, ApJ, 848, 88
Dainotti M. G., Del Vecchio R., Tarnopolski M., 2018, Advances in Astronomy, 2018, 4969503
Dainotti M., et al., 2019, arXiv e-prints, p. arXiv:1907.05074
Dainotti M. G., Lenart A. Ł., Sarracino G., Nagataki S., Capozziello S., Fraija N., 2020a, ApJ, 904, 97
Dainotti M. G., et al., 2020b, ApJ, 905, L26
Dainotti M. G., Lenart A. L., Sarracino G., Fernandez J., Nagataki S., Fraija N., Capozziello S., M. B., 2021a, Submitted to MNRAS
Dainotti M., Levine D., Fraija N., Chandra P., 2021b, Galaxies, 9, 95
Dainotti M. G., Lenart A. Ł., Fraija N., Nagataki S., Warren D. C., De Simone B., Srinivasaragavan G., Mata A., 2021c, PASJ, 73, 970
Dainotti M. G., et al., 2021d, ApJS, 255, 13
Dainotti M. G., De Simone B., Schiavone T., Montani G., Rinaldi E., Lambiase G., 2021e, ApJ, 912, 150
Dainotti M. G., Bargiacchi G., Lenart A. L., Capozziello S., Colgain E. O., Solomon R., Stojkovic D., Sheikh-Jabbari M., 2022a
Dainotti M. G., et al., 2022b, arXiv e-prints, p. arXiv:2203.12908
Dainotti M. G., De Simone B., Schiavone T., Montani G., Rinaldi E., Lambiase G., Bogdan M., Ugale S., 2022c, Galaxies, 10, 24
Del Vecchio R., Dainotti M. G., Ostrowski M., 2016, ApJ, 828, 36
Demianski M., Piedipalumbo E., Rubano C., Scudellaro P., 2012, MNRAS, 426, 1396
Demianski M., Piedipalumbo E., Sawant D., Amati L., 2017a, A&A, 598, A112

Demianski M., Piedipalumbo E., Sawant D., Amati L., 2017b, A&A, 598, A113
Eddington A. S., 1913, MNRAS, 73, 359
Efron B., Petrosian V., 1992, ApJ, 399, 345
Efstathiou G., 2020, arXiv e-prints, p. arXiv:2007.10716
Evans P. A., et al., 2009, Monthly Notices of the Royal Astronomical Society, 397, 1177
Fana Dirirsa F., et al., 2019, ApJ, 887, 13
Foreman-Mackey D., Hogg D. W., Lang D., Goodman J., 2013, PASP, 125, 306
Freedman W. L., 2021, ApJ, 919, 16
Freedman W. L., et al., 2020, ApJ, 891, 57
Frontera F., et al., 2018, Mem. Soc. Astron. Italiana, 89, 157
Gendre B., et al., 2013, arXiv e-prints, p. arXiv:1308.1001
Ghirlanda G., Ghisellini G., Lazzati D., 2004, ApJ, 616, 331
Ghirlanda G., Nava L., Ghisellini G., Firmani C., 2007, Astronomy & Astrophysics, 466, 127–136
Gompertz B. P., van der Horst A. J., O'Brien P. T., Wynn G. A., Wiersema K., 2015, MNRAS, 448, 629
Grupe D., Nousek J. A., Veres P., Zhang B.-B., Gehrels N., 2013, ApJS, 209, 20
Hu J. P., Wang F. Y., Dai Z. G., 2021, MNRAS, 507, 730
Kendall M. G., 1938, Biometrika, 30, 81
Khadka N., Ratra B., 2020, MNRAS, 499, 391
Khadka N., Ratra B., 2021a, arXiv e-prints, p. arXiv:2107.07600
Khadka N., Ratra B., 2021b, MNRAS, 502, 6140
Khadka N., Luongo O., Muccino M., Ratra B., 2021, J. Cosmology Astropart. Phys., 2021, 042
Khetan N., et al., 2021, A&A, 647, A72
Knust F., et al., 2017, A&A, 607, A84
Kocevski D., Butler N., 2007, in American Astronomical Society Meeting Abstracts. p. 18.01
Kodama Y., Yonetoku D., Murakami T., Tanabe S., Tsutsui R., Nakamura T., 2008, MNRAS, 391, L1
Kouveliotou C., Meegan C. A., Fishman G. J., Bhat N. P., Briggs M. S., Koshut T. M., Paciesas W. S., Pendleton G. N., 1993, ApJ, 413, L101
Lamb D. Q., 2003, AIP Conference Proceedings
Levan A., 2017, From the longest GRBs to the brightest supernovae, HST Proposal
Levan A. J., et al., 2007, MNRAS, 378, 1439
Leventis K., Wijers R. A. M. J., van der Horst A. J., 2014, MNRAS, 437, 2448
Levine D., Dainotti M., Zvonarek K. J., Fraija N., Warren D. C., Chandra P., Lloyd-Ronning N., 2022, ApJ, 925, 15
Li L., Wu X.-F., Lei W.-H., Dai Z.-G., Liang E.-W., Ryde F., 2018, ApJS, 236, 26
Liang E., Zhang B., 2005, ApJ, 633, 611
Lin W., Ishak M., 2021, J. Cosmology Astropart. Phys., 2021, 009
Lloyd N. M., 2000, in American Astronomical Society Meeting Abstracts. p. 25.06
Lü H.-J., Zhang B., Liang E.-W., Zhang B.-B., Sakamoto T., 2014, MNRAS, 442, 1922
Lü H.-J., Zhang B., Lei W.-H., Li Y., Lasky P. D., 2015, ApJ, 805, 89
Luongo O., Muccino M., 2020, A&A, 641, A174
Lusso E., et al., 2020, Astron. Astrophys., 642, A150
MacFadyen A. I., Woosley S. E., 1999, ApJ, 524, 262
MacFadyen A. I., Woosley S. E., Heger A., 2001, ApJ, 550, 410
Malmquist K. G., 1922, Meddelanden fran Lunds Astronomiska Observatorium Serie I, 100, 1
Mazets E. P., et al., 1981, Ap&SS, 80, 3
Norris J. P., Bonnell J. T., 2006, ApJ, 643, 266
Norris J. P., Gehrels N., Scargle J. D., 2010, ApJ, 717, 411
O'Brien P. T., Willingale R., 2007, Ap&SS, 311, 167
Oates S. R., et al., 2015, MNRAS, 453, 4121
Oates S., et al., 2017, Galaxies, 5, 4
Paczyński B., 1998, ApJ, 494, L45
Petrosian V., Kitanidis E., Kocevski D., 2015, ApJ, 806, 44
Piro L., Ricci R., Wieringa M., Bannister K., Troja E., Gendre B., Fiore F., Piranomonte S., 2014, ATCA observations of the new class of ultralong GRBs: a local proxy of popIII explosions?, ATNF Proposal
Postnikov S., Dainotti M. G., Hernandez X., Capozziello S., 2014, ApJ, 783, 126
Rea N., Gullón M., Pons J. A., Perna R., Dainotti M. G., Miralles J. A., Torres D. F., 2015, ApJ, 813, 92
Riess A., Anderson R. I., Breuval L., Casertano S., Macri L. M., Scolnic D., Yuan W., 2021, Uncrowding the Cepheids for an Improved Determination of the Hubble Constant, JWST Proposal. Cycle 1
Rodney S. A., et al., 2015, AJ, 150, 156
Rowlinson A., O'Brien P. T., Metzger B. D., Tanvir N. R., Levan A. J., 2013, MNRAS, 430, 1061
Rowlinson A., Gompertz B. P., Dainotti M., O'Brien P. T., Wijers R. A. M. J., van der Horst A. J., 2014, MNRAS, 443, 1779
Rowlinson A., Patruno A., O'Brien P. T., 2017, MNRAS, 472, 1152
Sakamoto T., et al., 2007, in American Astronomical Society Meeting Abstracts. p. 10.04
Scolnic D. M., et al., 2018, ApJ, 859, 101
Si S.-K., et al., 2018, ApJ, 863, 50
Srinivasaragavan G. P., Dainotti M. G., Fraija N., Hernandez X., Nagataki S., Lenart A., Bowden L., Wagner R., 2020, ApJ, 903, 18
Stratta G., Dainotti M. G., Dall'Osso S., Hernandez X., De Cesare G., 2018, ApJ, 869, 155
Tang C.-H., Huang Y.-F., Geng J.-J., Zhang Z.-B., 2019, ApJS, 245, 1
Torrado J., Lewis A., 2019, Astrophysics Source Code Library, p. ascl:1910.019
Torrado J., Lewis A., 2021, J. Cosmology Astropart. Phys., 2021, 057

Van Eerten H., 2014a, MNRAS, 442, 3495
Van Eerten H. J., 2014b, MNRAS, 445, 2414
Varela K., et al., 2016, A&A, 589, A37
Wang J. S., Wang F. Y., Cheng K. S., Dai Z. G., 2016, A&A, 585, A68
Wang X.-G., Zhang B., Liang E.-W., Lu R.-J., Lin D.-B., Li J., Lin L., 2018, The Astrophysical Journal, 859, 160
Wang F. Y., Hu J. P., Zhang G. Q., Dai Z. G., 2021a, arXiv e-prints, p. arXiv:2106.14155
Wang F., et al., 2021b, ApJ, 907, L1
Wei J., et al., 2016, arXiv e-prints, p. arXiv:1610.06892
Willingale R., et al., 2007, ApJ, 662, 1093
Woosley S. E., 1993, ApJ, 405, 273
Xu F., Tang C.-H., Geng J.-J., Wang F.-Y., Wang Y.-Y., Kuerban A., Huang Y.-F., 2020, arXiv e-prints, p. arXiv:2012.05627
Yonetoku D., Murakami T., Nakamura T., Yamazaki R., Inoue A. K., Ioka K., 2004, The Astrophysical Journal, 609, 935–951
Yu Y.-W., Zhu J.-P., Li S.-Z., Lü H.-J., Zou Y.-C., 2017, ApJ, 840, 12
Zhang B., Fan Y. Z., Dyks J., Kobayashi S., Mészáros P., Burrows D. N., Nousek J. A., Gehrels N., 2006, ApJ, 642, 354
Zhang B., et al., 2009, ApJ, 703, 1696
Zhao L., Zhang B., Gao H., Lan L., Lü H., Zhang B., 2019, ApJ, 883, 97

APPENDIX A: MONTE CARLO MARKOV CHAIN SAMPLING ERROR PREDICTION

In this section of the Appendix, we aim to quantify the numerical uncertainty that the MCMC sampling is inducing on the error on Ω_M. This will allow us to state that the errors provided on Ω_M in the text are at least one order of magnitude larger than the uncertainty on the MCMC sampling, thus confirming the reliability of the precision reached. We measure the numerical error introduced through *cobaya* MCMC sampling by monitoring the chain convergence using the Gelman-Rubin statistic (G-R). But even placing restrictions on both the G-R and its defined confidence level leaves some undefined uncertainties on the sampler-derived Ω_M and its error. Therefore, to make our results even more reliable, we loop all sampler runs 100 times until a Gaussian distribution of the inferred errors is produced to quantify those. From such, we derive the mean of both the Ω_M and its error, and these are the values which we report for all samples and combinations of samples. Two instances of this method are visualized in Fig. A1. To have a precise estimate of the σ associated with the error on Ω_M, we fit these distributions with a Gaussian curve and we superimpose the fit with a red line. We note that the error obtained by our simulation is smaller than the $\sigma = 0.0005$ of the errors of the distributions. This means that this fluctuation is one order of magnitude less than the uncertainties we are comparing in the main text.

When simulating additional GRBs, we control the numerical error innate to *emcee* by periodically computing the integrated auto-correlation time τ during sampling to manage the number steps taken. Because *emcee* uses parallel chains to reduce the variance, we can stop the sampling once the chains are longer than $\simeq 50\tau$ or 100τ. This method ensures that we generate the minimum number of samples to effectively reduce the relative error on our target integral. It is by these operations that we have confidence in not only our results, but also in their comparability between each other those by SNe Ia.

APPENDIX B: CHOOSING A POSTERIORI TRIM VALUES

In this Appendix section, we detail the selection of the a posteriori sample trim number of GRBs. For a number of observed GRBs in the interval between 10 and 25, we ran test simulations with 2300 simulated GRBs to determine the trend of the standard deviation on Ω_M for gradually increasing σ_{int} on the trimmed fundamental plane. This was performed for both optical and X-ray data, and with and without considering redshift evolution corrections. Fig. B1 shows the general trend for the PLAT (left panels) and OPT samples (right panels); each minimum shown both without (upper panels) and with (lower panels) accounting for redshift evolution is the number on which our a posteriori trim is based upon. Our reasoning here is that running the simulations for a wide range of trim choices would allow for a better choice of the number of GRBs to be used as the base for simulations, rather than determining this value a priori (before simulating). This idea is confirmed in Fig. B1 as we see that all of our a posteriori trims (minima) have significantly reduced uncertainties when simulated from our original choice of 10 GRBs indicated with the green solid line in all the panels determined by σ_{int} on their respective fundamental planes.

[h!]

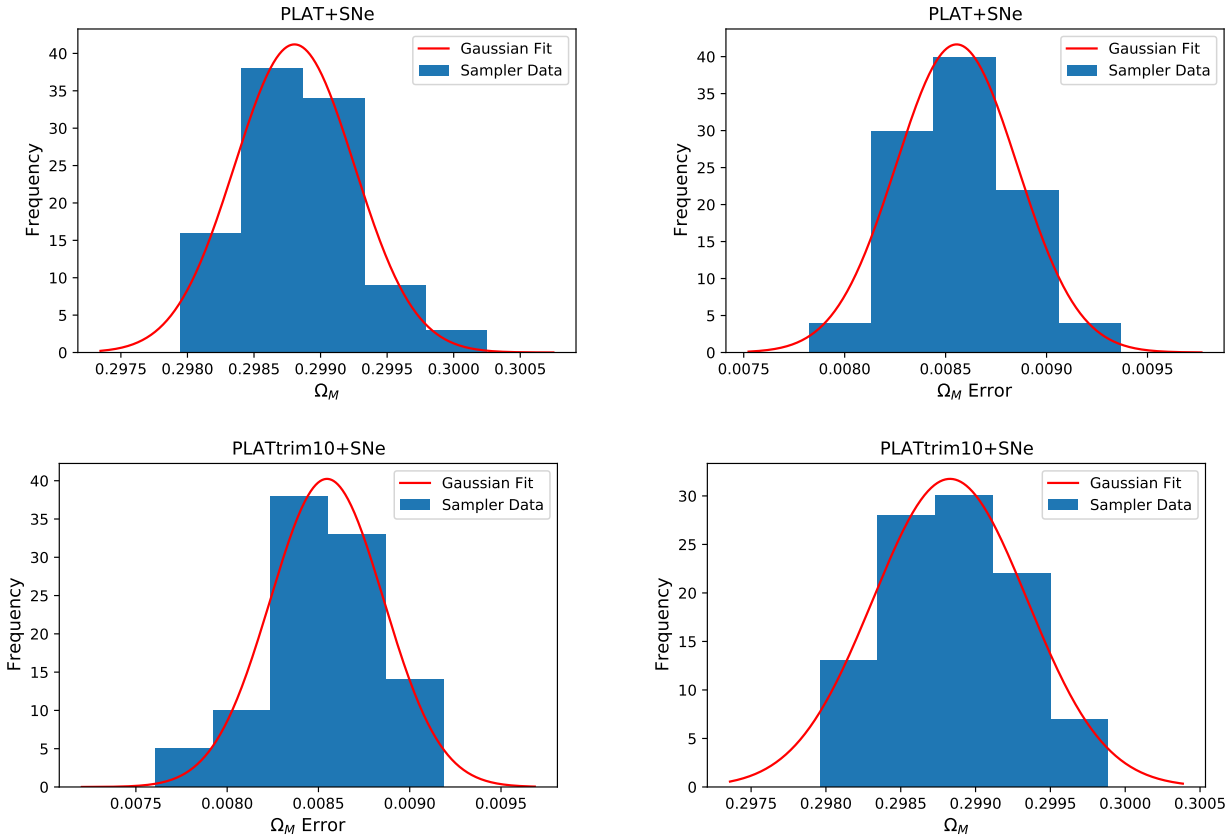

Figure A1. The two uppermost panels depict the MCMC sampler results for Ω_M (upper left) and its error (upper right) considering PLAT+SNe Ia probes together. The bottom panels show the same considering instead PLATtrim+SNe Ia probes. The PLATtrim sample in this Figure refers the apriori trim taken of the 10 GRBs closest to the fundamental plane.

[h]

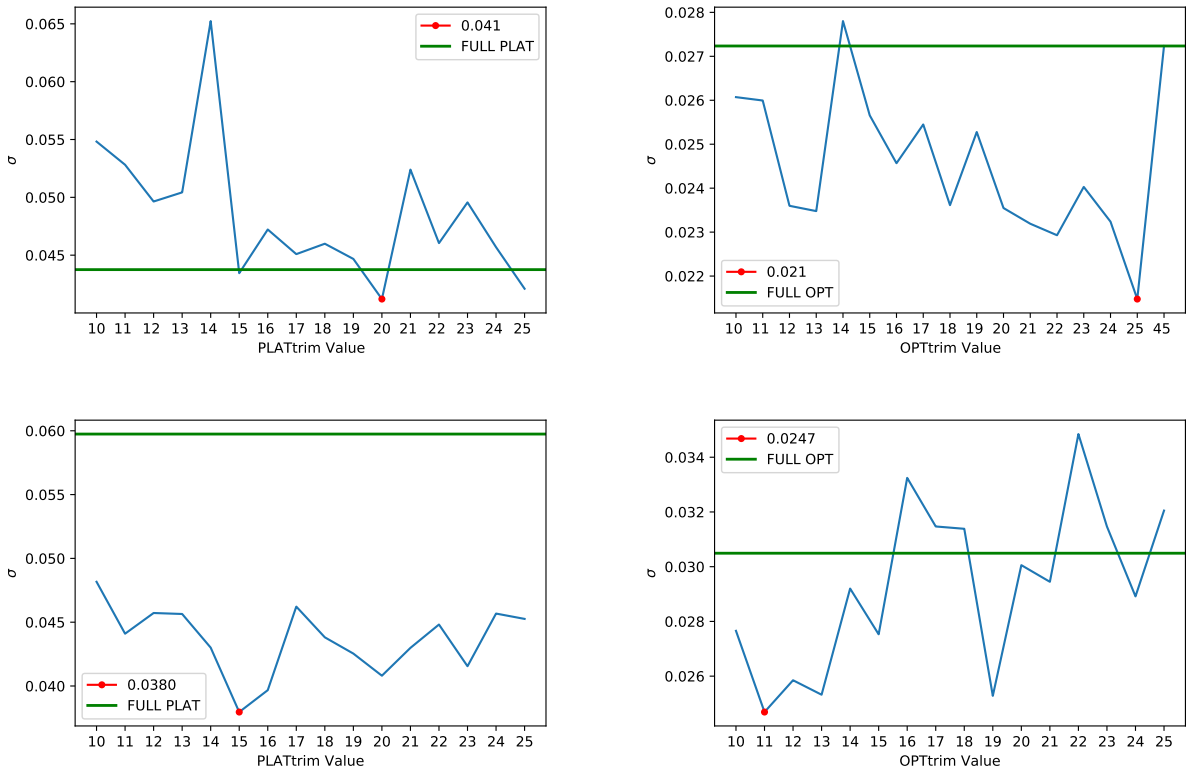

Figure B1. The leftmost plots in this Figure detail the trial simulations for varying PLATtrim values in the X-ray sample, whereas the rightmost plots do the same for varying OPTtrim in the Optical sample. The two upper panels do not consider redshift evolutionary effects; the bottom panels make corrections for both selection and redshift evolution biases.